Investigation of fast ion transport in TORPEX

A. Bovet, I. Furno, A. Fasoli, K. Gustafson and P. Ricci

École Polytechnique Fédérale de Lausanne (EPFL)
Centre de Recherches en Physique des Plasmas (CRPP)
Association Euratom-Confédération Suisse
CH-1015 Lausanne, Switzerland

E-mail: alexandre.bovet@epfl.ch

Abstract. Basic aspects of fast ion transport in ideal interchange-mode unstable plasmas are investigated in the simple toroidal plasma device TORPEX. Fast ions are generated by a miniaturized lithium 6+ ion source with energies up to 1 keV, and are detected using a double-gridded energy analyzer mounted on a two-dimensional movable system in the poloidal cross-section. The signal-to-noise ratio is enhanced by applying a modulated biasing voltage to the fast ion source and using a synchronous detection scheme. An analog lock-in amplifier has been developed, which allows removing the capacitive noise associated with the voltage modulation. We characterize vertical and radial transport of the fast ions, which is associated with the plasma turbulence. Initial experimental results show a good agreement with numerical simulations of the fast ion transport in a global fluid simulation of the TORPEX plasma.

PACS numbers: 52.55.Pi, 52.65.Cc, 52.25.Fi, 52.35.Ra, 52.40.Mj, 52.70.Nc

Submitted to: *Nuclear Fusion Special Issue : Energetic Particles "ENP11"*

1. Introduction

In burning plasmas, fast ions may be generated by ion cyclotron resonance heating (ICRH), neutral beam injection (NBI) and fusion reactions. As fast ions will be responsible for a significant fraction of plasma heating and, in some scenarios, non-inductive current drive, understanding their transport across the magnetic field is of fundamental importance. The interaction between highly energetic ions and small-scale (drift wave-like) turbulence is an open problem in fusion plasmas, which has not been extensively investigated to date. One of the reasons is that, in present tokamaks, fast ions do not play the same crucial role they will play in ITER [1]. Another, more fundamental, reason is that fast ions usually have a gyroradius larger than the turbulence scale, which weakens or almost entirely suppresses their interaction with turbulence by gyroaveraging effects [2, 3, 4]. A number of theoretical studies find that the interaction of fast ions with turbulence is reduced when the gyroradius is increased, while several

other authors demonstrate that, when the gyroradius increases up to the fluctuation correlation length, the fast ion transport could remain unchanged or even increase [5]. Recent tokamak results [6] indicate that significant redistribution of suprathermal ions can be induced by turbulence, at least in some ranges of energy and of the ratio between fast ion energy and background plasma temperature. Experimental indications of non-diffusive transport of fast ions in strong drift turbulence have been obtained in the linear basic plasma physics device LAPD at UCLA [7, 8]. So far, no direct measurements of turbulence-induced fast ion transport on toroidal devices have been performed. Thus, there exists a strong need for experimental data with which to compare and validate the relevant theoretical and numerical models [9, 10]. In this work, we investigate the interaction of fast ions with ideal interchange instabilities and turbulence in TORPEX simple magnetized toroidal plasmas, a relatively basic experimental environment with easy access for diagnostics and well-established plasma scenarios [11].

2. The TORPEX device and the interchange dominated plasma regime

The experiments are performed on the TORPEX device [11, 12, 13] (major radius R = 1 m, minor radius a = 0.2 m). Hydrogen plasmas are produced by microwaves (power $\approx$ 150 W) in the electron cyclotron range of frequencies on the high-field side of the torus. A vertical magnetic field $B_v = 2.1$ mT is imposed on a toroidal field of $B_t = 74$ mT, resulting in helical magnetic field lines with ∇B and curvature that terminate on the lower and upper walls of the vessel. Typical peak electron temperature and density are $T_e = 6$ eV and $n_e = 2 \times 10^{16}$ m^{-3} respectively. The vertical magnetic field line return distance is $\Delta = 2\pi R_0 B_v / B_t \approx 18$ cm. For fast ion transport measurements, signal-to-noise ratio is a concern, requiring TORPEX to be run in a continuous mode with plasma discharges lasting as long as 10 min. This allows for data acquisition of $\sim$ 30 s at each spatial position resulting in statistically relevant signals.

In the present configuration, experimental measurements [14] and numerical simulations [15, 16] reveal that plasma turbulence is dominated by an ideal interchange mode with frequency $f_p \simeq 4.5$ kHz and wave numbers $k_\parallel \simeq 0$ and $k_z \simeq 35$ m^{-1}. The ideal interchange mode is localized at the position of the steepest gradient of the density profile. This is shown by figure 1, which presents a snapshot of the density fluctuations and the time-averaged density profile measured by a two-dimensional array of 86 Lamgmuir probes, called HEXTIP [17]. A low-field side region, for $r \geq 0$, with negligible plasma production implying low densities and temperatures is characterized by the presence of radially propagating intermittent structures termed blobs [18, 19, 20, 21].

3. Experimental set-up: fast ion source and detector

The relatively low energy required for the fast ions (50eV- 1keV) allows a source design based on a miniaturized cylindrical structure (24mm in diameter, 50mm in length and an outlet diameter of 8mm), which can be installed directly inside the TORPEX vacuum

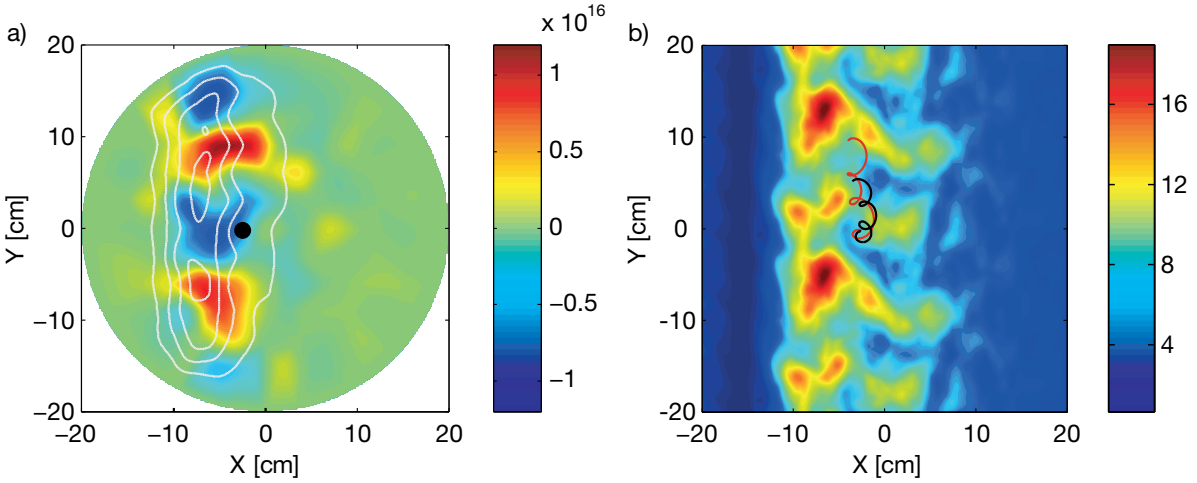

Figure 1. a) Poloidal cross-section of the electron density [m^{-3}] measured with the hexagonal Lamgmuir probe array HEXTIP. A snapshot of the fluctuations $\tilde{n} = n - \bar{n}$ is represented in the background and the white lines show the isocontours of the time averaged density $\bar{n}$. The black dot indicates the position of the fast ions source. b) Snapshot of the simulated turbulent electrostatic field [V]. Two example trajectories of fast ions with energies of 88 eV (black) and 290 eV (red) are over-plotted.

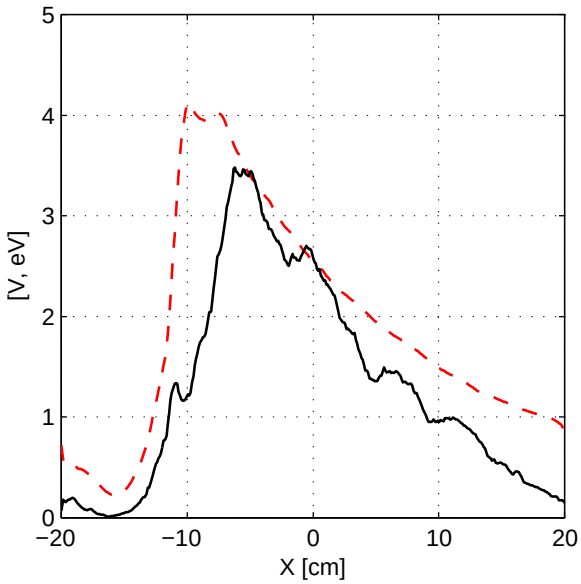

Figure 2. Profiles of electron temperature and floating potential fluctuations from the 2D simulations. (- - - -) Vertical average of T_e, (——) $\sigma_{V_{float}}$ on the midplane

vessel [22, 23]. The source consists of a thermionic emitter with a two-grid accelerating system and produces fast ion currents up to 10μA.

A miniaturized gridded energy analyzer (GEA) is used to measure fast ion energy and current density profiles. To improve the signal to noise ratio, a design with two identical gridded energy analyzers facing opposite directions was chosen [24]. The ad-

vantage of this configuration is that one detector measures the fast ion beam together with the background signal while the second detector measures only the background noise. Each fast ion detector has small dimensions (15mm in diameter, 70mm in length and in inlet diameter of 8mm), and is able to measure fast ion currents as small as 0.1μA. The fast ion source and the double gridded energy analyzer are installed on 2D moving systems, which can position them at almost any point of the poloidal cross-section. The 2D moving detector system is motorized and allows automatic reconstruction of the fast ion current density profile with a spatial resolution of $\sim$ 5mm.

Synchronous detection is used in order to increase the signal-to-noise ratio [24]. The emitter bias is modulated by a reference signal at a given frequency ($\sim$ 1 kHz). This modulation results in undesired space-dependent capacitively coupled noise in the detector. In order to remove this parasitic effect, an analog lock-in amplifier has been developed. Before demodulation by the lock-in, the detector signal is modified to remove capacitive effects by introducing a "dead time" which erases the spurious capacitive cusp in the signal. The final signal is then integrated to obtain a DC output proportional to the fast ion current.

4. Theoretical interpretation framework

The TORPEX plasma has been subject to extensive modeling, including validation of a global plasma turbulence code [14]. These simulations have been performed in 2D and 3D limits of the drift-reduced Braginskii fluid equations, adapted to the TORPEX geometry and plasma parameters [15, 16]. As mentioned above, these simulations have confirmed that TORPEX plasmas are dominated by ideal interchange modes for certain values of the ratio B_v/B_t. This is the case for all plasmas studied in this paper. For a theoretical understanding of the fast ion transport in this turbulent regime, we take the simulated turbulent electrostatic field and integrate the trajectories of a large ensemble of tracer particles using the full Lorentz force. Therefore, these fast ion simulations explicitly include the charge and mass of the Li-6 ions, as well as the geometry of the toroidal magnetic field, which effectively causes curvature and ∇B drifts. Gyroaveraging is also included implicitly to high accuracy with this method. Figure 1 shows a snapshot of the simulated turbulent electrostatic field with the trajectories of two fast ions overplotted.

A comprehensive theoretical study of the behavior of the fast ions as tracer particles was recently completed [9, 10]. These results show that the dispersion of fast ions in the plane perpendicular to the magnetic field is generally nondiffusive, with $\sigma_R^2(t) \sim t^\gamma$, where $\gamma \neq 1$. Here, $\sigma_R^2(t) = \langle (R - \langle R \rangle)^2 \rangle$ where R is the ions radial position. A large number of different ensembles of fast ions was used to explore the variations of the value of γ as a function of two dimensionless quantities: the fast ion energy compared to the electron temperature, $\mathcal{E}/T_e$, and the amplitude of turbulent fluctuations relative to the electron temperature. It was seen that, depending on the value of these parameters, the

value of γ can go from superdiffusive ($\gamma > 1$) to subdiffusive ($\gamma < 1$) due to the effects of gyroaveraging and, more significantly, curvature-drift averaging.

An example of the behavior of the radial dispersion of the fast ions, $\sigma^2(t)$, as a function of time is shown in figure 7. One can see that the Larmor oscillation dominates at the beginning of the injection, during the so-called ballistic phase. Then, after approximately one gyroperiod, the plasma interaction becomes most significant. Ideally, to measure γ and distinguish between different injection energies and positions, a 3D profile of the fast ion current density should be measured. As of now, a well-resolved 2D profile is available for four different injection energies. With this initial data, it is already possible to compare the measurements from the gridded energy analyzer with the simulated data.

5. Experimental results and comparisons with theory

We conduct a first set of experiments with four fast ion energies from 88 eV to 290 eV. The source is positioned at X_0 = -2.5 cm and Y_0 = -0.25 cm (figure 1), with a slight downward tilt relative to the horizontal plane. Source and detector are separated toroidally by 23 degrees, corresponding to 40 cm. At the injection position, the standard deviation of the floating potential time series and the electron temperature average over time and vertical position are $\sigma_{V_{f0}} \simeq 2$ V and $T_{e0} \simeq 3$ eV, respectively. We note that, in similar plasma conditions as those studied here, the fluctuation level of V_{float} and of the plasma potential, ϕ, have been found to be of similar amplitudes [25]. The fast ion current profile is reconstructed from several discharges, for which the spatial resolution of the measurements is adapted to the profile. The adaptive resolution varies typically from 5mm near the peak position to 1 cm at approximately 2 cm from the peak. Profiles of the fast ion current density are then computed by interpolating the scattered measurement points over a regular grid with a resolution of 1 mm.

First, a measurement of the fast ion beam with neither magnetic field nor plasma is performed to extract the source orientation and the initial spreading of the beam. Then, profiles with and without plasma are reconstructed for energies of 88 eV, 142 eV, 190 eV and 290 eV. The experimental profiles of the fast ion current are shown in figure 3. In this configuration, the fast ion cyclotron frequency is $f_{fi} = \Omega_{fi}/2\pi \simeq 188$ kHz and the fast ions perform from 0.8 to 1.5 Larmor gyrations before they encounter the detector for energies of 88 eV to 290 eV respectively. Over this range of energies, the fast ion Larmor radii, calculated from the source orientation and initial spreading, vary between $\rho_{fi} \simeq 0.58 \pm 0.22$ cm for 88 eV to $\rho_{fi} \simeq 1.05 \pm 0.40$ cm for 290 eV. The vertical shift of the center of the fast ion distribution is due to a combination of the ion Larmor motion and the drifts induced by curvature and gradient of the magnetic field.

To perform the simulations of the fast ions trajectories, the background and turbulent $\mathbf{E}$ field are numerically modeled with the 2D code introduced in section 4 using the experimental parameters. Simulations are performed with different values

of the particle and heat sources to match the experimental temperature profile. The simulated profiles of electron temperature and floating potential fluctuations are shown in figure 2. The positions of the maxima of T_e and of the V_{float} fluctuations correspond to the positions of the experimental density peak and of the mode shown in figure 1. The value of the floating potential fluctuations is slightly higher in the simulation than in the experiment. As in experiments, fluctuation levels of V_{float} and ϕ are of very similar amplitude. Thus, in order to match potential fluctuations, the simulated plasma potential fluctuations, $\tilde{\phi} = \phi - \bar{\phi}$, are multiplied by a factor $\Xi = 0.7$ [9, 10]. The simulation time is $t_{sim} = 200/\Omega_{fi}$, which represents $\sim 75\%$ of the interchange wave period.

All initial parameters of the fast ion injection, namely, position, energy and orientation, are modeled with a Gaussian distribution. Fast ions are injected at the location of the fast ion source (X_0 = -2.5 cm, Y_0 = -0.25 cm). The standard deviation of the position distribution is $\sigma_{X_0,Y_0} = 1.2$ mm. The standard deviation of the initial energy distribution corresponds to 10% of the initial energy. Values of the vertical, α_0, and horizontal, β_0, angles describing the source orientation and angular size can be deduced from the profile reconstructed from the case without magnetic field. However, owing to the sensitivity of the trajectories upon theses initial parameters, simulations were run in order to find a single pair of initial angles that provides an agreement with the positions of the experimental peaks for all relevant energies. Values of α_0 = -0.1 rad and β_0 = -0.1 rad give the best match and are consistent with measurements made without magnetic field within the experimental spatial accuracy. The spreading in initial angles is $\sigma_{\alpha_0} = 0.06$ rad and $\sigma_{\beta_0} = 0.04$ rad.

Comparisons between experiment and simulation are done using a synthetic diagnostic allowing the poloidal cross section of the fast ion current density to be computed (figure 4). The synthetic diagnostic reproduces the technique used by the experimental diagnostic. First, the poloidal cross section is divided into bins with a size of 5mm×5mm, and then, the fast ion current resulting from the passage of all particles is computed in each bin. Finally, the resulting fast ion current profile is interpolated with a resolution of 1 mm.

The positions of the peaks in the cases without plasma show a good agreement with the data, within the experimental spatial accuracy, for all energies (figures 3 and 4). The profiles are all broadened by the plasma, meaning that the interaction of the fast ions with the plasma is significant. A simple estimate of the effect of ion/fast ion collisions on the beam spreading shows that collisional spreading is an order of magnitude smaller than our observation. The radial and vertical full width at half maximum (FWHM) for different energies is computed by slicing the profiles horizontally and vertically each millimeter. Only the slices with a maximum value higher than the half value of the total peak are taken into account. In figure 5, the average over the different slices is used and the errorbars are given by the standard deviation. Comparison of the profiles radial and vertical FWHM also show a good agreement. The effect of the plasma is more

important for lower energies for both radial and vertical FWHM. The radial FWHM first decreases as the energy is increased up to 190 eV and then increases again at 290 eV for the cases with plasma, as well as without plasma. This oscillation of the beam width can be explained by the gyromotion of the fast particles. Indeed, the difference in the initial phases of the fast ions is very small and their Larmor motion is almost synchronized resulting in a oscillation of the beam width at the cyclotron frequency and with an amplitude of the Larmor radius on top of the gyrocenter dispersion.

Figure 6 shows the FWHM^2 computed with the synthetic diagnostic for all energies as a function of the toroidal distance. The square of the standard deviation of the particle positions as a function of time, $\sigma^2(t)$, is also shown in figure 7. A ballistic phase, whose length corresponds approximately to the distance traveled during the first gyromotion, is present for all energies. Then, a smooth transition occurs to a second phase, the interaction phase, where the effect of the plasma begins to be important. Exponents characterizing the transport in the interaction phase are computed from the slope of the log-log plots using $\mathrm{FWHM}^2 \sim L^{\gamma'}$, where L is the toroidal distance. Here, γ'_R is the radial transport exponent and γ'_z is the vertical transport exponent. The radial transport exponent is decreasing as energy increases up to 190 eV indicating that the transport becomes more subdiffusive and increases again slightly at 290 eV. The values of γ'_z increases slightly as energy increases, from 0.8 to 1.0. The values of γ'_z and γ'_R show the same trend than the values of γ_R and γ_z extracted from the plots of $\sigma^2(t)$ (figure 7). However, they are systematically smaller. Indeed, in the presence of nondiffusive transport, the measure of the FWHM does not capture the non-Gaussian tails of the fast ion distribution, whereas the standard deviation, σ, does.

The values of γ_z extracted from the plots of $\sigma^2(t)$ are all above unity indicating a superdiffusive transport in the vertical direction consistent with theoretical estimates [9, 10]. The values of γ_R are all below unity, indicating that the radial transport is subdiffusive. As energy increases, γ_R first decreases as expected from [9, 10], however from 190 eV to 290 eV, γ_R increases again. This disagreement with the results in [9, 10] can be explained by the nonparallel injection used in the present work. Nonparallel injection introduces a transient dispersion phase for larger values of fast ion injection energy. This transient phase is characterized by a larger γ_R value relative to theoretical predictions [9, 10], which becomes larger for higher injection energies. This subdiffusive γ_R is seen in the distribution of ion displacements as a wider peak without much lengthening of the tails. The transient phase ends after several tens of Larmor rotations, after which the value of γ_R conforms with theoretical predictions for parallel injection. We have identified non-parallel injection as a necessary condition for the presence of the transient phase.

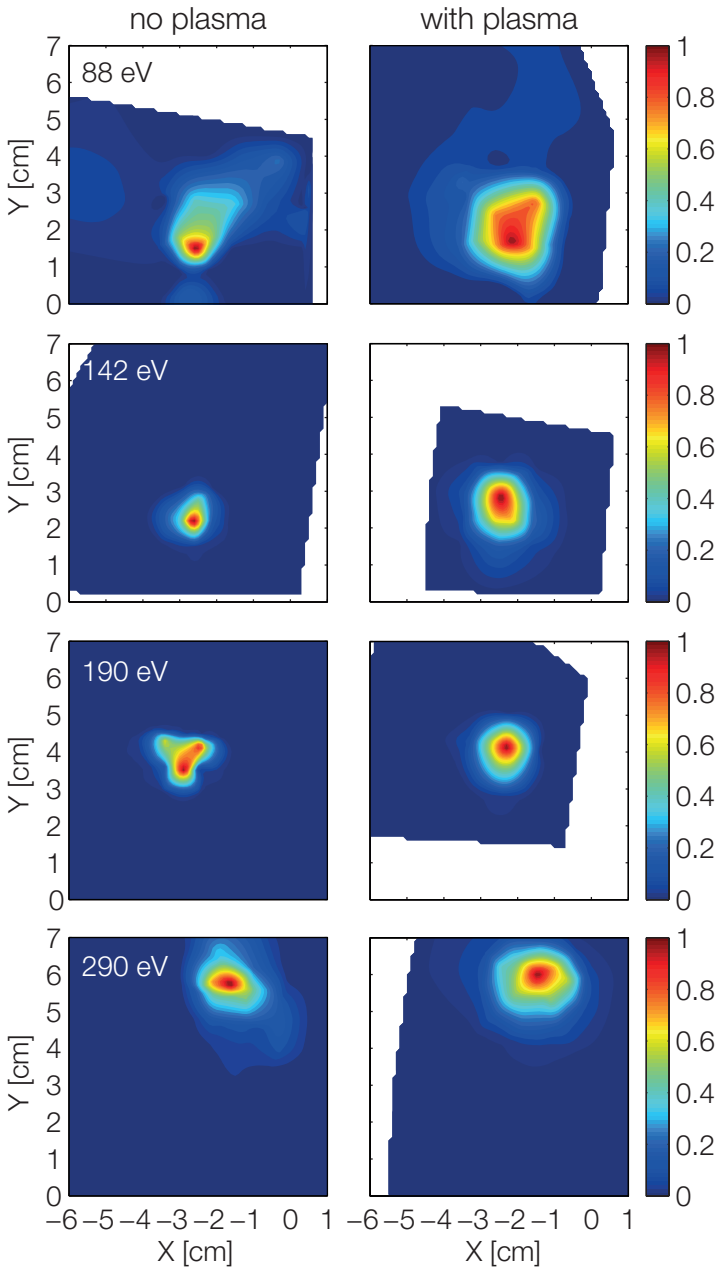

Figure 3. Fast ion experimental current density profiles (a.u.) measured at 40cm from the fast ion source with energies ranging from 88eV (top) to 290eV (bottom). Cases without plasma are on the left and cases with plasma on the right. The current density values of each plot is normalized to its maximum.

6. Conclusions and outlook

First experimental results on the spatial distribution of supra-thermal ions in simple magnetized plasmas show a significant effect from ideal interchange waves and turbulence. This effect is well explained by simulations, showing the importance of the size of the gyroradius. In order to resolve the oscillations of the beam due to gyromotion of the fast ions and discriminate among different mechanisms of fast ion transport, a

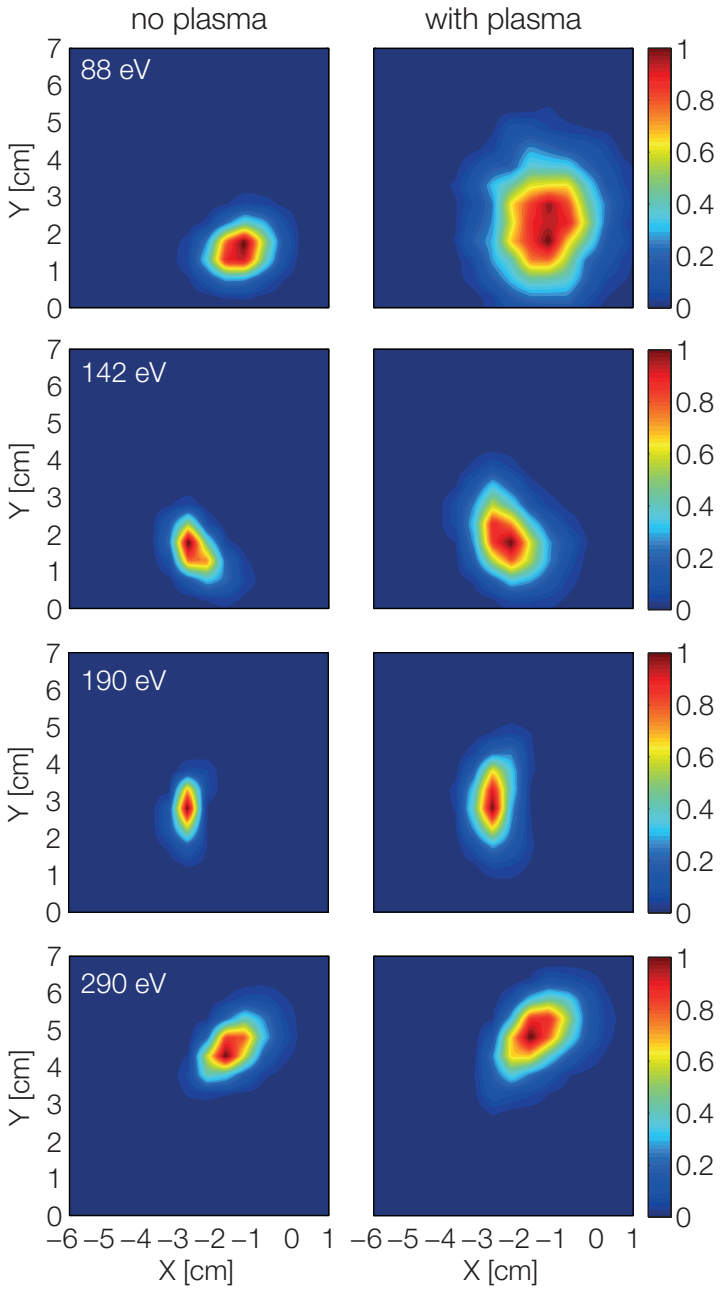

Figure 4. Fast ion current density profiles (a.u.) reconstructed from the simulations with a synthetic diagnostic. Fast ion energy vary from 88eV (top) to 290eV (bottom). Cases without plasma are on the left and cases with plasma on the right. The current density values of each plot is normalized to its maximum.

toroidally moving system for the source has recently been developed (figure 8). This system will allow continuous variation of the distance between the source and the detector to reconstruct 3D profiles of the fast ion beam in the ballistic and interaction phases. Taking into account the machine size and the vertical drift experienced by the fast ions, we expect the maximum distance between the source and the detector to be approximately 2.5 m for 300 eV ions. This would result in a number of gyrations

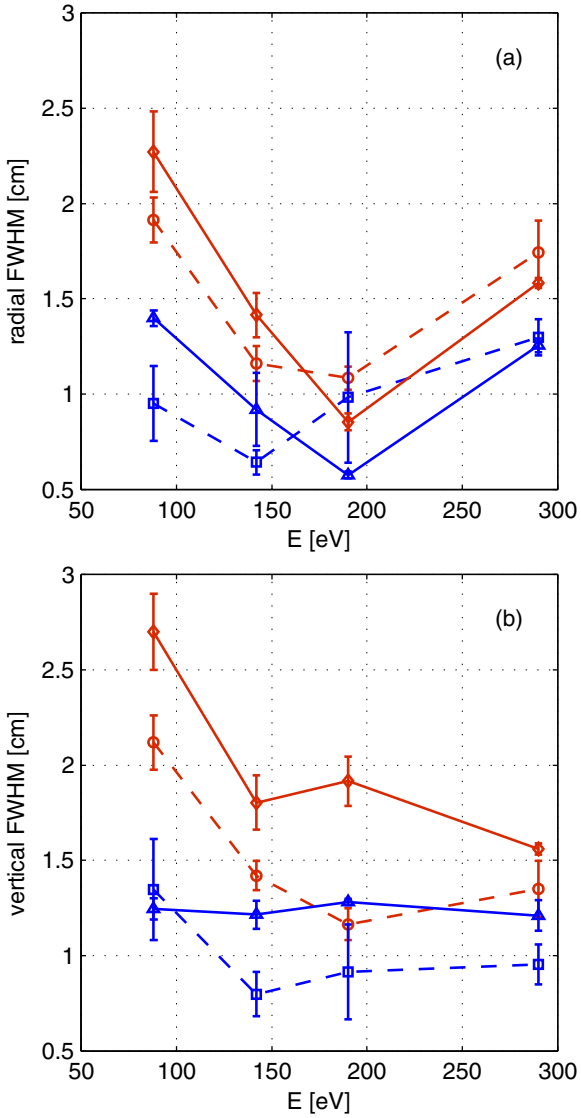

Figure 5. Full width half maximum of the fast ion beam profiles from experiment (- - - -) and simulations (——). The cases without plasma are in blue and the cases with plasma are in red. (a) radial FWHM, (b) vertical FWHM.

between 5 and 9, for energies between 88 eV and 290 eV. In order to increase the number of gyrations before collection by the detector, the injection angle can also be increased.

Transport of fast ions in the presence of well-diagnosed waves and turbulence will be investigated by varying, for example, the fast ion energy to temperature ratio, the initial pitch angle, and the turbulence characteristics. Different magnetic configurations will be used, from the SMT described here to one with rotational transform induced by an internal current carrying wire. This toroidal experimental setup, combined with the numerical simulations resolving the individual fast ion tracer trajectories, will allow us to investigate the guiding-center treatment and the effect of the gyroaveraging and curvature-drift averaging relevant to large fusion devices.

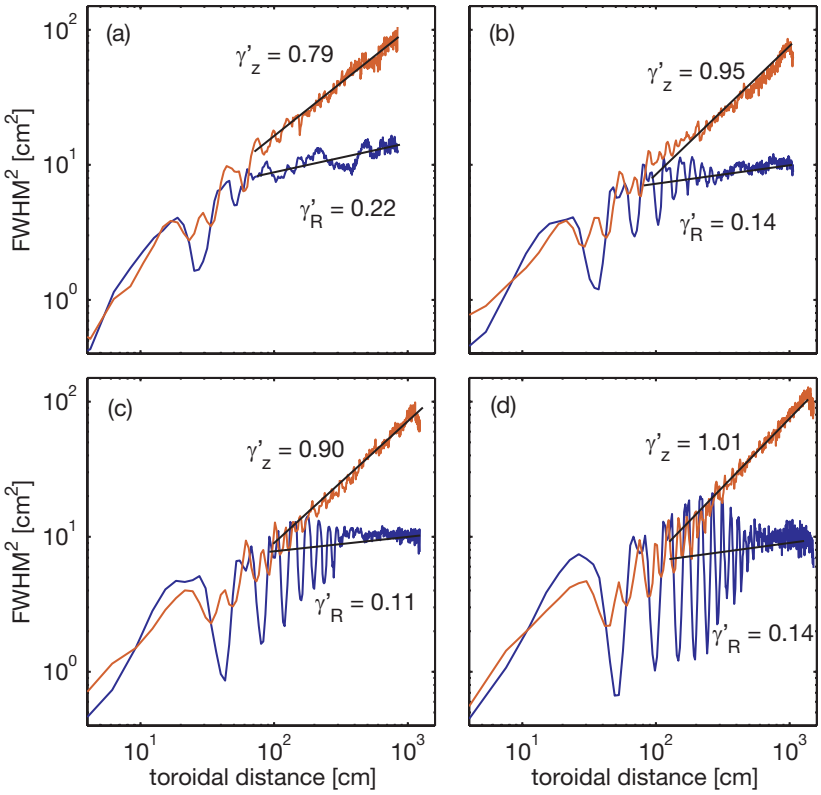

Figure 6. FWHM^2 as a function of the toroidal distance reproduced with the synthetic diagnostic for E = 88 eV (a), 142 eV (b), 190 eV (c) and 290 eV (d). Radial FWHM^2 is in blue and vertical FWHM^2 is in red. Values of the radial and vertical transport exponents extracted from the slopes of the plots are displayed.

Acknowledgments

We acknowledge helpful discussions with Christian Theiler. This work was supported in part by the Swiss National Science Foundation.

References

[1] A Fasoli, C Gormenzano, H L Berk, B Breizman, S Briguglio, D S Darrow, N Gorelenkov, W.W Heidbrink, A Jaun, S.V Konovalov, R Nazikian, J.-M Noterdaeme, S Sharapov, K Shinohara, D Testa, K Tobita, Y Todo, G Vlad, and F Zonca. Chapter 5: Physics of energetic ions. *Nuclear Fusion*, 47(6):S264–S284, June 2007.

[2] H Naitou, T Kamimura, and J M Dawson. Kinetic Effects on the Convective Plasma Diffusion and the Heat Transport. *Journal of the Physical Society of Japan*, 46(1):258–265, January 1979.

[3] W W Heidbrink and G J Sadler. The behaviour of fast ions in tokamak experiments. *Nuclear Fusion*, 34:535, 1994.

[4] G Manfredi and R Dendy. Test-Particle Transport in Strong Electrostatic Drift Turbulence with Finite Larmor Radius Effects. *Physical Review Letters*, 76(23):4360–4363, June 1996.

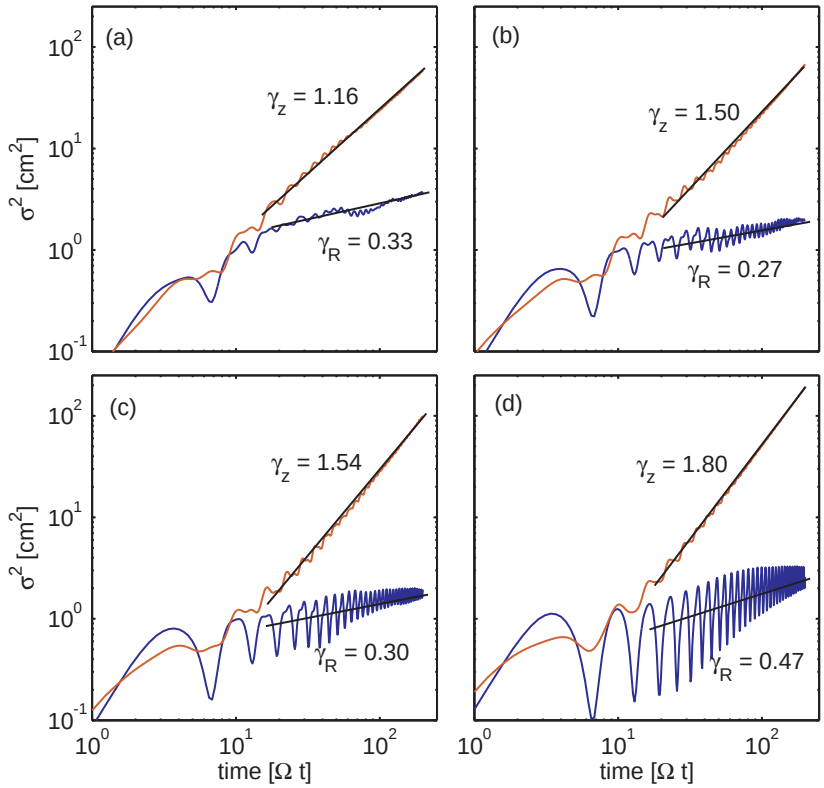

Figure 7. Here we show σ^2 as a function of time for E = 88 eV (a), 142 eV (b), 190 eV (c) and 290 eV (d). Radial σ^2 is in blue and vertical σ^2 is in red. Values of the radial and vertical transport exponents extracted from the slopes of the plots are displayed.

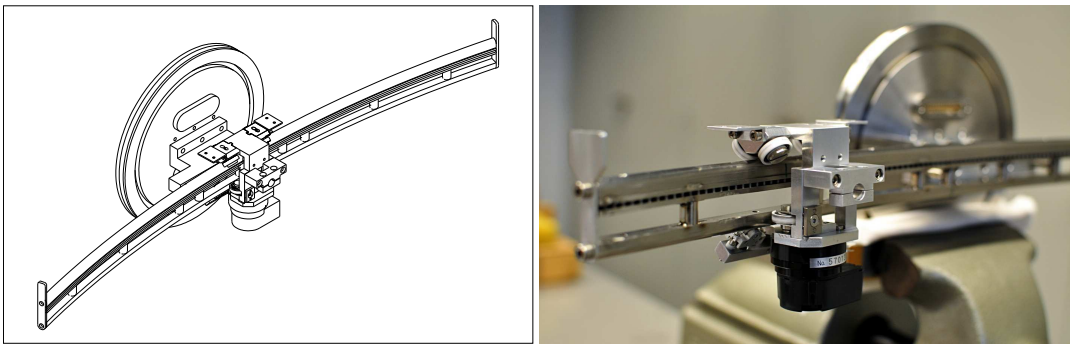

Figure 8. Schematic and picture of the movable system which will allow the fast ion source to move over 60 cm toroidally.

[5] T Hauff and F Jenko. Mechanisms and scalings of energetic ion transport via tokamak microturbulence. *Physics of Plasmas*, 15(11):112307, November 2008.

[6] S Günter, G Conway, S DaGraça, H-U Fahrbach, C Forest, M. Garcia Muñoz, T Hauff, J Hobirk, V Igochine, F Jenko, K Lackner, P Lauber, P McCarthy, M Maraschek, P Martin, E Poli, K Sassenberg, E Strumberger, G Tardini, E Wolfrum, H Zohm, and Asdex Upgrade Team. Interaction of energetic particles with large and small scale instabilities. *Nuclear Fusion*, 47(8):920–928, August 2007.

[7] S Zhou, W W Heidbrink, H Boehmer, R McWilliams, T Carter, S Vincena, S K P Tripathi, P Popovich, B Friedman, and F Jenko. Turbulent transport of fast ions in the Large Plasma Device. *Physics of Plasmas*, 17(9):092103, 2010.

[8] S Zhou, W W Heidbrink, H Boehmer, R McWilliams, T A Carter, S Vincena, and S K P Tripathi. Dependence of fast-ion transport on the nature of the turbulence in the Large Plasma Device. *Physics of Plasmas*, 18(8):082104, 2011.

[9] K Gustafson, P Ricci, I Furno, and A Fasoli. Nondiffusive suprathermal ion transport in simple magnetized toroidal plasmas. *Physical Review Letters*, 108:035006, Jan 2012.

[10] K Gustafson, P Ricci, A Bovet, I Furno, and A Fasoli. Fast ion turbulent transport in simple magnetized torus configurations. *submitted to Physics of Plasmas*.

[11] A Fasoli, B Labit, M McGrath, S H Müller, G Plyushchev, M Podestá, and F M Poli. Electrostatic turbulence and transport in a simple magnetized plasma. *Physics of Plasmas*, 13(5):055902, 2006.

[12] A Fasoli, A Burckel, L Federspiel, I Furno, K Gustafson, D Iraji, B Labit, J Loizu, G Plyushchev, P Ricci, C Theiler, A Diallo, S H Mueller, M Podestà, and F Poli. Electrostatic instabilities, turbulence and fast ion interactions in the TORPEX device. *Plasma Physics and Controlled Fusion*, 52(12):124020, December 2010.

[13] S Müller, A Fasoli, B Labit, M McGrath, O Pisaturo, G Plyushchev, M Podestà, and F M Poli. Basic turbulence studies on TORPEX and challenges in the theory-experiment comparison. *Physics of Plasmas*, 12(9):090906, 2005.

[14] P Ricci, C Theiler, A Fasoli, I Furno, K Gustafson, D Iraji, and J Loizu. Methodology for turbulence code validation: Quantification of simulation-experiment agreement and application to the TORPEX experiment. *Physics of Plasmas*, 18(3):032109, 2011.

[15] P Ricci and B N Rogers. Three-dimensional fluid simulations of a simple magnetized toroidal plasma. *Physics of Plasmas*, 16(9):092307, 2009.

[16] P Ricci and B N Rogers. Turbulence Phase Space in Simple Magnetized Toroidal Plasmas. *Physical Review Letters*, 104(14):1–4, April 2010.

[17] S H Müller, A Diallo, A Fasoli, I Furno, B Labit, G Plyushchev, M Podestà, and F M Poli. Probabilistic analysis of turbulent structures from two-dimensional plasma imaging. *Physics of Plasmas*, 13(10):100701, October 2006.

[18] C Theiler, I Furno, A Fasoli, P Ricci, B Labit, and D Iraji. Blob motion and control in simple magnetized plasmas. *Physics of Plasmas*, 18:55901, 2011.

[19] A Diallo, A Fasoli, I Furno, B Labit, M Podestà, and C Theiler. Dynamics of Plasma Blobs in a Shear Flow. *Physical Review Letters*, 101(11):10–13, September 2008.

[20] M Podestà, A Fasoli, B Labit, I Furno, P Ricci, F M Poli, A Diallo, S H Müller, and C Theiler. Cross-field transport by instabilities and blobs in a magnetized toroidal plasma. *Physical Review Letters*, 101:045001, Jul 2008.

[21] I Furno, B Labit, A Fasoli, F M Poli, P Ricci, C Theiler, S Brunner, A Diallo, J P Graves, M Podestà, and S H Müller. Mechanism for blob generation in the torpex toroidal plasma. *Physics of Plasmas*, 15(5):055903, 2008.

[22] G Plyushchev. *Interaction of supra-thermal ions with turbulence in a magnetized toroidal plasma*. PhD thesis, Lausanne, 2009.

[23] Y Zhang, H Boehmer, W W Heidbrink, R McWilliams, D Leneman, and S Vincena. Lithium ion sources for investigations of fast ion transport in magnetized plasmas. *Review of scientific instruments*, 78(1):013302, January 2007.

[24] G Plyushchev, A Diallo, A Fasoli, I Furno, B Labit, S H Müller, M Podestá, F M Poli, H Boehmer, W W Heidbrink, and Y Zhang. Fast ion source and detector for investigating the interaction of turbulence with suprathermal ions in a low temperature toroidal plasma. *Review of Scientific Instruments*, 77(10):10F503, 2006.

[25] C Theiler, I Furno, A Kuenlin, Ph Marmillod, and A Fasoli. Practical solutions for reliable triple probe measurements in magnetized plasmas. *Review of scientific instruments*, 82(1):013504,

January 2011.